



## Protection of Strategic Concrete Structures from the effects of Blast Loads

Ahmed Gomaa<sup>1</sup>\*, Amr Riad<sup>2</sup>, Mohamed Abd el-Razik<sup>3</sup>.

<sup>1</sup>Structural design engineer works for Moharam Bakhoum Consulting Engineers.

<sup>2</sup>Prof. of Reinforced Concrete –Faculty of Engineering -Al-Azhar University.

<sup>3</sup>Prof. of Reinforced Concrete –Faculty of Engineering -Al-Azhar University

\* Correspondence: E-mail: [Eng.a.s.gomaa@gmail.com](mailto:Eng.a.s.gomaa@gmail.com).

### الملخص العربي :

تناقش هذه الورقة شرحا موجزا لمدى الحماية المقدمة لمبنى استراتيجي مهم وهو المنشآت الخرسانية المسلحة لصوامع الحبوب . ركزت الدراسات السابقة إما علي تقييم الحالة الهيكلية لصوامع الخرسانة المسلحة بعد تعرضها للانفجارات أو دراسة تأثير الانفجارات الداخلية على الجدران دون مراعاة عوامل أخرى مثل الجوانب المعمارية والتشغيلية والطوبوغرافية. تهدف الدراسة إلى مناقشة انتشار موجات الانفجار التي تؤثر على المقطع الأفقي للصوامع الخرسانية المسلحة ليكون محور دراسة ثلاثية الأبعاد بناء على متغيرات مختلفة بما في ذلك متغير الصلابة وحالة ملء للصومعة ونوع الركيزة. تم محاكاة وتحليل نماذج عديدة متعددة باستخدام برنامج الـ ANSYS في هذه الدراسة لتقييم تأثير موجات الانفجار على صومعة الخرسانة المسلحة. تم مناقشة مخرجات محاكاة الـ Ansys بيانيا من خلال: (1) انتشار موجة الانفجار (2) تركيز الضغط المنعكس (3) أقصى انحراف (4) أقصى ضغط منعكس . تم استخدام هذه النتائج لدراسة العوامل المؤثرة على الصوامع وتوفير تدابير حماية إضافية للصومعة ضد موجات الانفجار. تم إستنتاج أن استخدام هذه المعلمات يلعب دورا حيويا في تقليل تأثير حمل الانفجار على صوامع الخرسانة المسلحة .

### Abstract:

This paper discusses a brief explanation of the protection extent provided for an important strategic building (i.e., the reinforced concrete structures of grain silos). Past studies focused on either evaluating the structural condition of the Reinforced Concrete silos after undergoing explosions or studying the impact of internal explosions on the walls without considering other factors such as architectural, operational, and topographical aspects. The study aims to discuss the Blast-waves propagation affecting the horizontal section of reinforced concrete silos and choosing the optimal section design to be the focus of a 3D study based on different variables including the stiffness variable, silo filling state, type of structural support. Multiple numerical models have been simulated and analyzed by using the ANSYS program in this study to evaluate the Blast-waves' effect on the reinforced concrete silo. Ansys simulation outputs area reflected graphically through: 1) Blast-wave propagation 2) Concentration of reflected pressure 3) Maximum deflection 4) Maximum reflected pressure. These graphical results are used to study the affecting factors on the silos and

provide extra protection measures for the silo against Blast-waves. It was concluded that using these parameters plays a vital role in decreasing the blast load effect on RC silos.

**Keywords:** Reinforced concrete silo; Blast load; Reflected pressure; variable Stiffness.

## 1. Introduction

The protection of strategic structures has a significant impact on providing economic stability in countries, and in light of the exacerbation of the threat of terrorism, it was necessary to study this. Such protection can be provided by improving the structural characteristics of the building or using various materials capable of withstanding high dynamic loads (blast load). But there are some other parameters that can be controlled to provide more economic and practical solutions, these parameters will be discussed in this paper. Previous studies studied the effect of explosive loads on concrete structures from different aspects. The description of the phenomenon of the explosion was of great interest. David Comie et al [1] The blast wave was explained as a transient air pressure wave created by a rapid chemical reaction. As a result, the wavefront emanates from the explosive charge Centre in a hemispheric form. The maximum overpressure value is influenced by the distance between the explosive charge and the target (i.e., the pressure above normal air pressure). Kinney and Graham [2] The explosion was defined as "a natural phenomenon caused by a sudden release of energy. Ngo, et al [3] defined the explosion as a large-scale, rapid, and unexpected release of energy. To study the blast wave propagation, Johnson, et al [4] investigated the varied ranges of pressure waves produced by spherical, cubic, cylindrical, and tetrahedral explosive charge specimens to see how they affected energy expansion. High-speed imaging was used to track the shock wave and its effects. Gebbeken [5] provided a brief overview of blast wave propagation and reflection. Various architectural approaches have been found to be beneficial in reducing the impact of explosions. Králik [6] compared an empirical formula for dealing with explosive waves to the numerical computation of the AUTODYN algorithm taking in consideration the presence of solid barriers in front of structure, It was concluded that solid barriers have a major impact on the pressure wave. Temsah [7] analyzed the Beirut explosion by utilizing nonlinear numerical modelling of finite elements to investigate the structural state of existing silos and the level of damage caused by the explosion. The volume of total blast waves distributed by the Beirut explosion silos was found to be weak, and the silos' current structural condition was found to be unsafe. M. Chiquito [8] investigated Blast impacts on structural elements (concrete beams and floors) and other construction materials (i.e., masonry panels). All structural elements were subjected to 16 separate large-scale tests, which were created and assessed. The test data was used for digital modelling and damage assessment, and it was shown that numerical modelling of these tests can be used to predict future scenarios and analyses threats under similar conditions. Schenker [9] Largescale field blast testing was conducted on shielded and unshielded concrete slabs. The experiment has aimed to (1) extract data on the original

concrete structure's dynamic reaction to blasting loads for verification and validation (V&V) of associated computer algorithms, and (2) validate the efficiency of aluminum foams in reducing blast wave loads. Multiple layers of aluminum foam were shown to be useful in providing enough protection after repeated field blast testing on shielded and unprotected concrete slabs. Schenker successfully obtained time-dependent measurements of the target's responses to blast wave loads. Ismail [10] did a 3D scan of Beirut's port silos to evaluate the extent of the damage. Because of the limited space at Beirut Port, ABAQUS FEA was used to quantify the explosion's strength and determine whether the pile foundation could be utilized for the construction of new silos. Earth and foundations have played a positive role by absorbing some of the energy and reducing the energy emitted by the explosion. [11-14] The relationship between the change in pressure disturbance and time is shown in Figure 1. The value of the ambient pressure remains consistent until time "t<sub>A</sub>," after which there is a sudden and rapid increase in pressure until it reaches the "peak over-pressure (P<sub>so</sub>)". The overpressure value rapidly declines as explosion waves spread, reaching ambient pressure at the moment "t<sub>A</sub> + t<sub>o</sub>," which is known as "The positive phase". The "negative phase" follows, in which the air pressure is lower than the ambient pressure. Returning to ambient pressure takes longer than the previous phase, as measured by "t<sub>A</sub> + t<sub>o</sub> + t<sub>o</sub><sup>-</sup>" time.

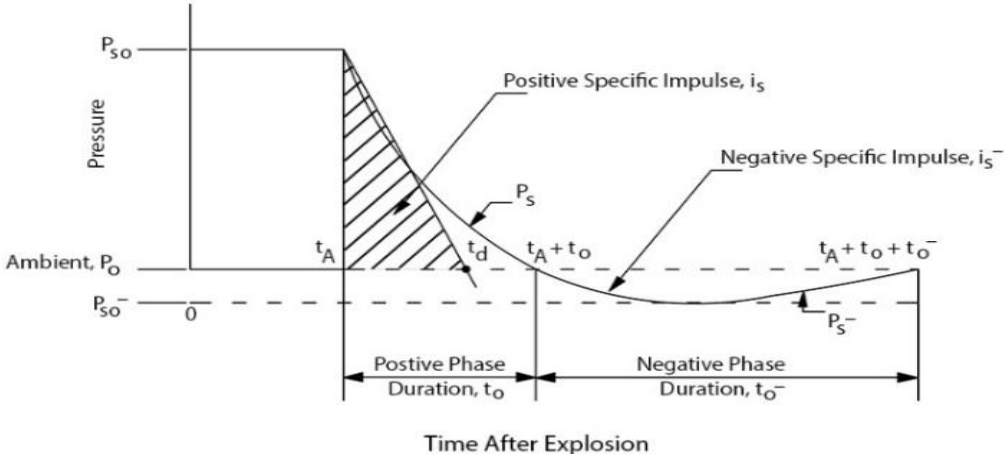


**Figure 1.** Free-Field Pressure-Time Variation. [11-14]

The blast wave outputs, which are critical for structural loading, were explained. The peak of the overpressure at the wave-front (P<sub>so</sub>) is the area integration under the combined pressure-time curve during the positive phase (i<sub>s</sub>), as illustrated in Figure 1, and its equation is:

$$i_s = \int P_s(t) dt \dots \dots \dots (1)$$

[15] In equation (2) Friedlander discussed "Blast-wave pressure profiles" through the "Friedlander exponential equation" where (b) is the wave parameter.

$$P_{(t)} = p_s \left[ 1 - \frac{t}{t_o} \right] \exp \left\{ -\frac{b t}{t_o} \right\} \dots \dots \dots (2)$$

For many uses, however, the approximations are quite satisfactory. Variation of overpressure with time is often therefore approximated by a linear decay, the duration is called ( $t_d$ ). Therefore, ( $i_s$ ) can be calculated from the approximate area of the semi triangular area beneath the curve Figure 1, by using this equation:

$$i_s = \frac{1}{2} t_d p_s \dots \dots \dots (3)$$

and therefore, the value of ( $t_d$ ) can be calculated through the following equation:

$$t_d = \frac{2i_s}{p_s} \dots \dots \dots (4)$$

**2. Modeling of Blast interaction.**

The ANSYS workbench tool allows you to present a realistic model that is required for this case study's simulation and analysis. As a result, the model's components and their relationships must be addressed as follows:

**2.1 Blast Source Modeling:**

The explosive materials are represented by their properties that affect the explosion outputs, as shown in equation No. (5) which is known as the Jones-Wilkins- Lee (JWL) equation [16, 17]. The equations used by the ANSYS workbench program to describe the state of the explosion source are a result of a series of experimental programs their development follows an earlier equation proposed by Jones and Miller and an equation developed by Wilkins.

$$P_{(\Delta)} = Ae^{-R_1 \cdot V} + Be^{-R_2 \cdot V} + \frac{C}{V^{\omega+1}} \dots \dots (5)$$

V stand for the relative volume  $\frac{v}{v_0}$ , following the coefficients used in ANSYS. Substitution of  $V_{SP}$  (specific volume), and  $\rho_0$  (Loading density), V will convert those expressions to a specific volume. The pressures given are in megabars (Mbar) unit, and the parameters are abbreviated as  $\Delta$ , A, B, R1, R2 and are presented in Figure 2.

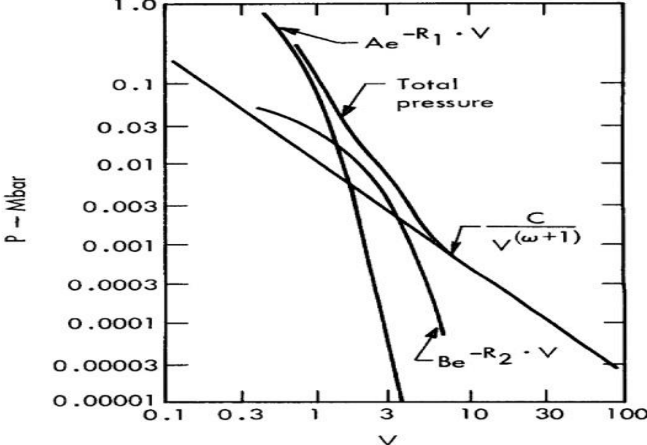


**Figure 2.** Contribution of various terms in JWL equation of state to total ambient pressure for Composition B, Grade A [16, 17].

**2.2 Space Modeling.**

The dimensions in which the explosion occurs are known as (space). The explosion's outputs are directed at the target. (Space) was proven to be air in this investigation, and EOS (equation of state) for air was clarified as follows:

a) Air has EOS of Ideal Gas [18] with its material properties as shown in Eq. (6).

$$P = (\gamma - 1)\rho \cdot e + P_{shift} \dots \dots \dots (6)$$

Where  $\gamma$  is the adiabatic exponent,  $\rho$  is the density of air,  $e$  is internal air energy, and  $P_{shift}$  is a small initial pressure defined to give a zero-starting pressure.

b) The method of connecting and transferring for the output : The various digital processors in the ANSYS workbench (ANSYS 2019) use finite differences and finite volume approaches in most cases. This technique allows for the selective use of different numerical processors in modelling distinct components and regimes of different problems. Individually organized meshes controlled by these numerical processors can be connected in space and time to calculate structural issues, fluid dynamics, and gas dynamics, as well as coupled problems (for example fluid Structure, gas structure, structure-structure, etc.). The Lagrange processor for modelling solid continua and structure, Euler processors for modelling fluids, gases, and large distortion, ALE (Arbitrary Lagrange Euler) processor for specialized flow models, and Shell processor for modelling thin structural elements are all included in the ANSYS workbench.

**2.3 Target Modeling.**

The goal in this stage of our study is reinforced concrete modeling and therefore a representation of its components must be studied. The previous studies stated that the definition of concrete behavior under the influence of high-speed dynamic stresses are represented by two aspects: a) Description of the porosity of concrete EOS model. b) Definition of concrete's compressive strength by RHT model. This can be explained as the follows:

a) EOS Concrete Model.[19] Figure 3 shows how the pore crush pressure and compaction pressure are important in the volumetric compaction model. The model becomes elastic at a pressure equal to the pore crush pressure. When pore collapse occurs, the associated micromechanical effects reduce the volumetric stiffness of the material, resulting in a significant drop in the effective bulk modulus. The material's porosity is represented by an internal variable that indicates the ratio of the matrix material's density to the density of the porous concrete.

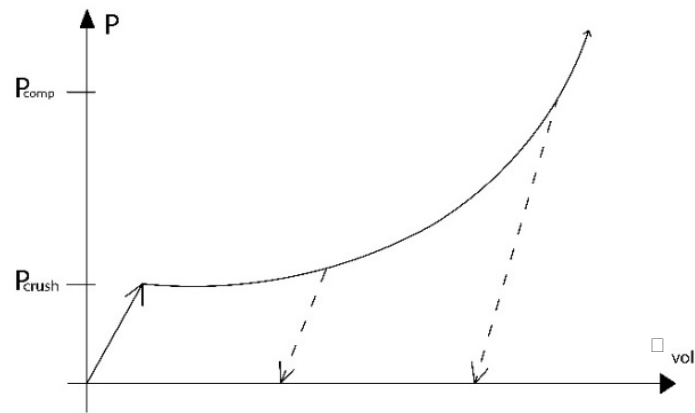


**Figure 3** Schematical description of the  $p$ - $\alpha$  equation of state [19].

**b) The RHT Concrete Model.** [20] The initial elastic yield surface, the failure surface, and the residual friction surface are the three stress limit surfaces in the Riedel-Hiermaier-Thoma (RHT) concrete model. Figure 4 shows the static compressive meridian surfaces. The strength reduction along the different meridians is explained by the surfaces as well as strain rate effects. The failure surface, or ultimate strength of the concrete, is determined by material properties such as the concrete's compressive, tensile, and shear strengths. The initial yield surface is then created through user-input of percentages of the failure surface along the tensile and compressive meridian.

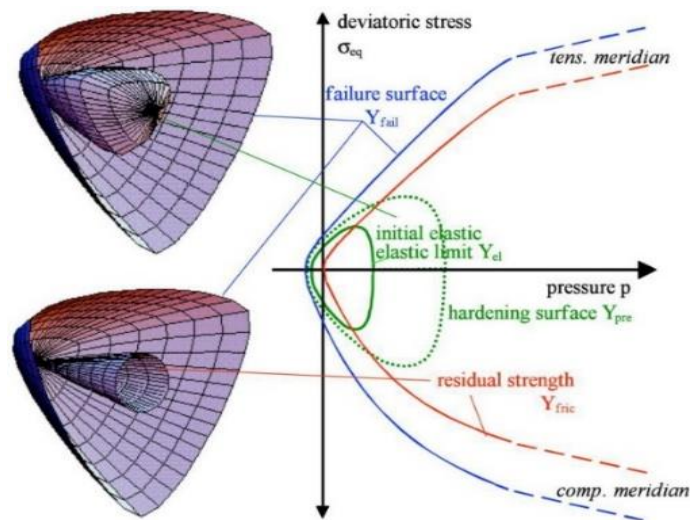


**Figure 4** Three surface concept for the concrete strength with hardening, failure and residual friction. [20]



represents the height of the materials inside the silo and "H" represents the silo's free height. The only difference between the two groups was the form of support, which was separated into fixed and hinged support groups.

## 4. Model Data

### 4.1 Geometry

The Configuration of the groups, which were chosen for the study, are presented in Table 1. Figure 5. illustrates typical dimensions for all models.

### 4.2 Material Properties.

All material properties and EOS (Equation of State) were obtained from ANSYS workbench Materials Library. Air, TNT, Concrete 35 MPa, and Steel 420 MPa were used for the numerical modeling and simulation. Other settings or parameters that are not mentioned here are set to default values by ANSYS workbench code. Lagrange processor was applied for modeling solid continua and structures, while Euler processor was applied with the multi-material flow for modeling fluids, gases, and large distortions. Erosion and Failure were applied to see distortion phenomena in Lagrange models.

### 4.3 Boundary conditions and load conditions.

The effect of the blast waves on reinforcement concrete silo was simulated in finite element to give the same behavior in nature. Therefore, two types of supports have been assumed to study the response of the concrete silo to the compressive waves.

The first type is fixed support in which the silo walls are completely attached to the base to prevent horizontal, vertical, and rotational movement. The second type is hinged support which is assumed to be identical to the hinged support of the frame to allow rotation, and prevent horizontal and vertical movement. Figure 6 shows the shape of the fixed and hinged support.

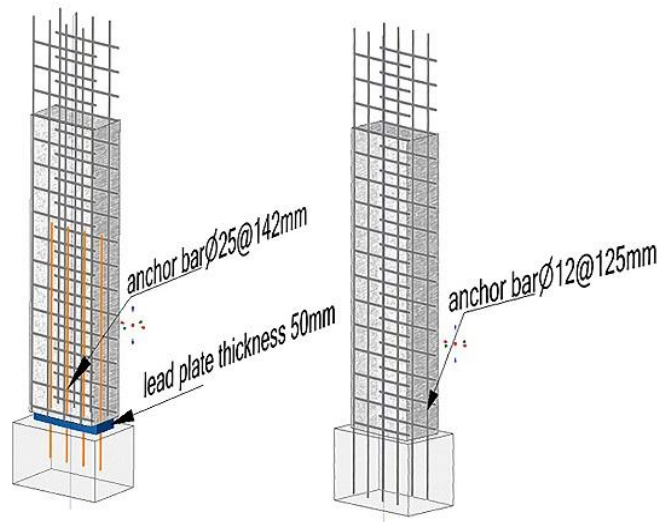


**Figure 6.** General Support Systems (fixed & hinged base)

**Table 1.** Standard limits for all samples of RC silos.

Standard limits for all samples																	
Case	NO. G	TNT				S.O.D (m)											
		Truck vehicle		1000 KG		10											
Study Cases	I. Geometric shape	Group 2	S01	Circular													
			S02	Square													
			S03	Diamond													
			S04	Rectangle													
			S05	Oval													
			S06	Hexagon													
	II. Variable stiffness	Group 1	Fixed	NO. S	T.O. S	Dimension			K	Z	V	%R					
						10	30	D (m)	t <sub>w</sub> cm	H(m)	I/H		L/H	R/H			
								S01	5	21.4	Empty		Flat	0°			
								S02	10	10.7							
								S03	15	7.1							
								S04	20	5.4							
								S05	25	4.3							
		S06	30	3.6													
		S07	35	3.1													
		Group 2	Hinged	NO. S	T.O. S	Dimension			K	Z	V	%R					
						10	30	D (m)	t <sub>w</sub> cm	H(m)	I/H		L/H	R/H			
								S01	5	21.4	Empty		Flat	0°			
								S02	10	10.7							
S03	15							7.1									
S04	20							5.4									
S05	25	4.3															
S06	30	3.6															
S07	35	3.1															
III. Filling & unloading	Group 1	Fixed	NO. S	T.O. S	D (m)	t <sub>w</sub> cm	H(m)	K	Z		%R						
									10	30		35	3.1	L/H			
														S01	0%	Flat	0°
														S02	14%		
														S03	29%		
														S04	43%		
														S05	57%		
														S06	71%		
	S07	86%															
	S08	100%															
	Group 2	Hinged	NO. S	T.O. S	D (m)	t <sub>w</sub> cm	H(m)	K	Z		%R						
									10	30		35	3.1	L/H			
														S01	0%	Flat	0°
														S02	14%		
S03														29%			
S04														43%			
S05	57%																
S06	71%																
S07	86%																
S08	100%																

T.O. S(i.e., Type of supporting system). NO. S (i.e., Number of Samples). S.O.D(i.e., Stand of distance). D (i.e., Inner diameter of the silo). NO. G (i.e., Number of Group). t<sub>w</sub> (i.e., wall thickness of silo).

## 5. Analysis of Results.

The following analysis results will be discussed: the Blast-wave propagation, the concentration of reflected pressure, the maximum deflection, and the maximum reflected pressure. The study results are graphically represented.

$\delta_{\max}$  and  $P_{r\max}$  were chosen as comparison points between the studied samples to evaluate the impact of blast load on the reinforced concrete silo, where  $\delta_{\max}$  value of deflection at time  $2.18\text{e-}3$  sec and  $P_{r\max}$  is the maximum reflected pressure value measured on the front facade of the silo.

### 5.1 Case study No. I Geometric shape.

Figure 7. illustrates the distributed explosion waves on different cross-sections of the silo. By monitoring distributed explosion waves behavior around the shapes, it was noticed that the curvature of the silo's section shape has a significant impact on the waves flowing extent around cross-sections. The more convex the silo cross-section is, such as circular or oval-shaped, the more it has the ability to penetrate waves without a high rise in the reflected pressure, unlike cross-sections with large confrontation areas, such as rectangular or square-shaped. Distributed explosion waves of silos with hexagon-shaped cross-sections are the most accepted amongst the various shapes previously mentioned.

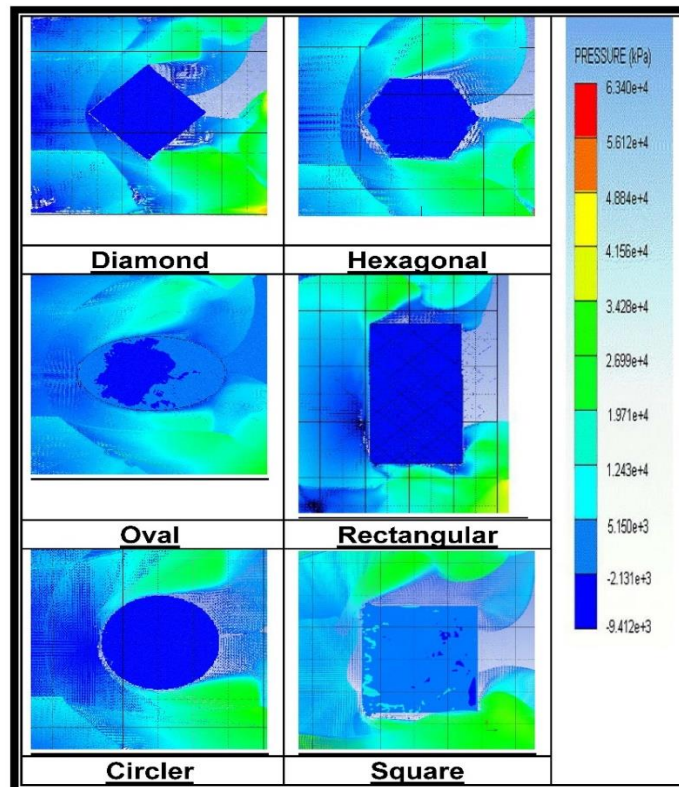
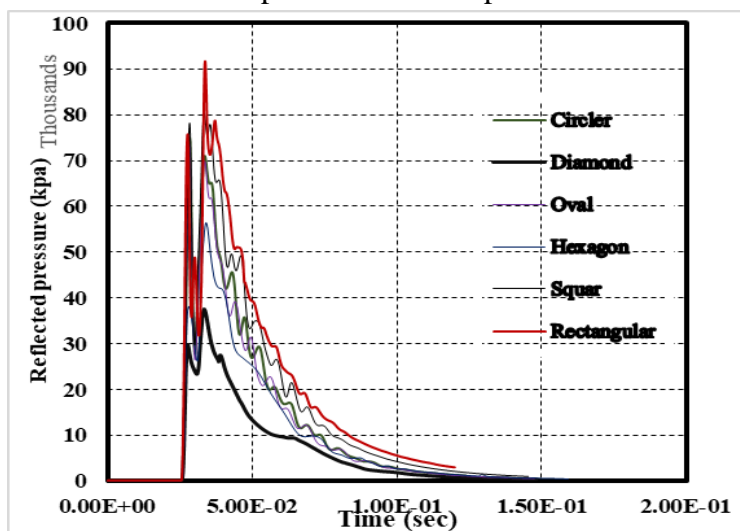


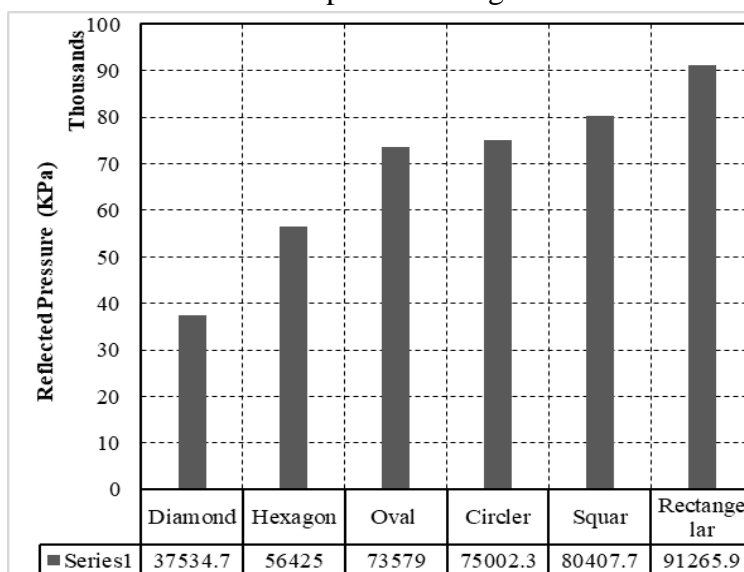
Figure 7. Propagation of blast wave around sample cross-sections.

Figure 8. discusses the reflected pressure values at point "a" (i.e., the closest point on the shape's perimeter to the TNT explosive charge), where it shows the highest value of the reflected pressure to the section with large confrontation areas, such as rectangular and square, unlike what happened to more convex sections. An inversely proportional relationship was noticed between convexity and reflected pressure value, where the Diamond-shaped cross-section had the lowest reflected pressure value at point "a".



**Figure 8.** Comparison of reflected pressure-time curves for all point a (i.e., which is the closest point on the perimeter of the shape to the explosive charge).

The more the shape's convexity and curvatures, such as circle and oval and hexagonal cross-sections, the less the values are. Check a comparison in Figure 9.



**Figure 9.** Comparison of reflected pressure for all shapes at point a (i.e., which is the closest point on the perimeter of the shape to the explosive charge).

## 5.2 Case study II. Variable stiffness.

This case was concerned with the study of the effect of the variable stiffness of the concrete section of the silos on the comparison points mentioned above for Group1 and Group2, which are similar in stiffness variable K but with different support, type fixed and hinged respectively.

### 5.2.1. Analysis result of II.V-G1.

Figure 10. illustrates the relationship between  $\delta_{\max}$  (i.e., the maximum deflection at time 2.18E-3 sec) and the K-modulus. The curve has been divided into three phases, which determined to what extent the variable stiffness affects the deflection of the RC silo. The first phase is the region in which the K value ranges from 21.4 to 7.2. Despite the large disparity in the K value, the  $\delta_{\max}$  change was small. This first phase represents samples S01 to S03. The second phase represents samples S03 to S06, and in this phase, there is a noticeable increase in  $\delta_{\max}$  values with the changeover of K values.

The third phase represents the remainder of the samples, noticed that the rate of change between K and  $\delta_{\max}$  of this stage is the most eminent, meaning that a small increase in the value of K leads to a marked increase in the value of the maximum deflection of RC silo. The value of the deviation  $\delta_{\max}$  at the time of 2.18E-3 sec & K, chosen for the study, as shown in Table 2

**Table 2.** Values of Max. deflection  $\delta_{\max}$  at time 2.18E-3 sec and Stiffness modulus K for Group 1.

No. O. S	K	Time (sec)	$\delta_{\max}$ (mm)
II.V-G1-S01	21.40	2.18E-03	11.695
II.V-G1-S02	10.70	2.18E-03	11.82
II.V-G1-S03	7.10	2.18E-03	11.795
II.V-G1-S04	5.40	2.18E-03	12.104
II.V-G1-S05	4.30	2.18E-03	12.323
II.V-G1-S06	3.60	2.18E-03	12.625
II.V-G1-S07	3.10	2.18E-03	13.389

NO. S (i.e., Number of Samples).

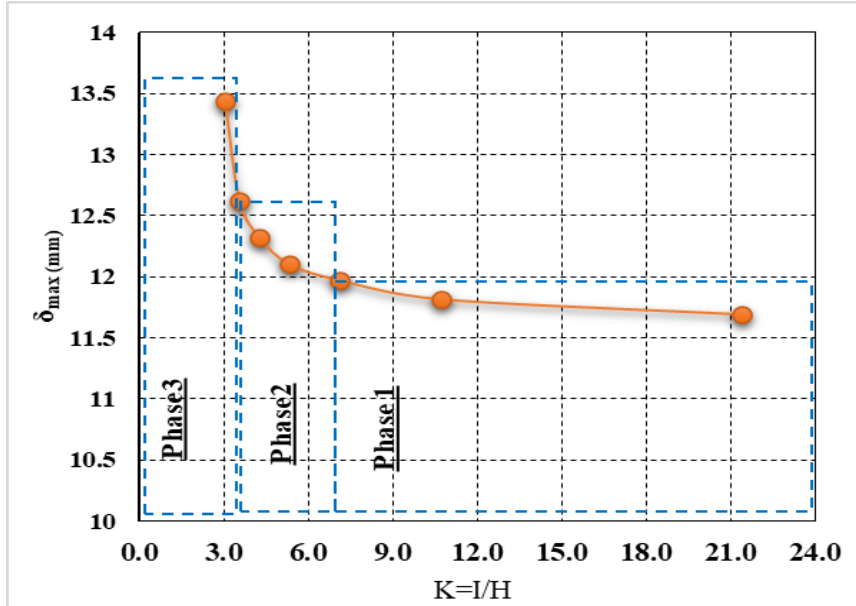


**Figure 10.** Relationship between K (i.e., Stiffness modulus) &  $\delta_{max}$  (i.e., Max. deflection (mm)) of Group1.

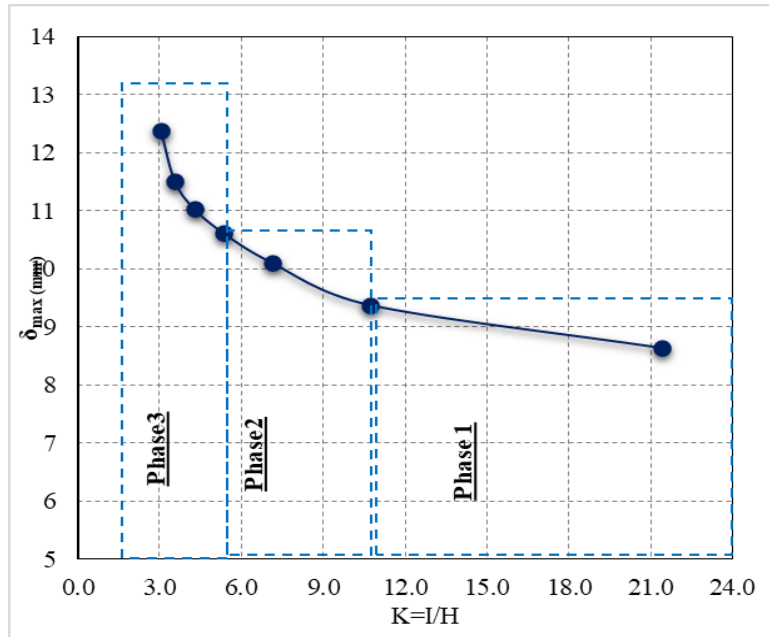
### 5.2.2. Analysis result of II.V-G2.

Figure 11. illustrates the relationship between  $\delta_{max}$  (i.e the maximum deflection at time  $2.18E-3$  sec) and the K-modulus. The curve has been divided into three phases, which determined to what extent the variable stiffness affects the deflection of the RC silo. The first phase is the region in which the K value is from 21.4 to 10.70 despite the large disparity in the K value, the  $\delta_{max}$  change was small, and the first phase represents samples S01 to S02. The second phase represents samples S02 to S05, and in this phase, there is a noticeable increase in  $\delta_{max}$  values with the changeover of K values. The third phase represents the remainder of the samples, noticed that the rate of change between K and  $\delta_{max}$  of this stage is the most eminent, meaning that a small increase in the value of K leads to a marked increase in the value of the maximum deflection of RC silo. The value of the deviation  $\delta_{max}$  at the time of  $2.18E-3$  sec & K, chosen for the study, will be shown in Table3.

**Table 3.** Values of Max. deflection  $\delta_{max}$  at time  $2.18E-3$  sec and Stiffness modulus K for Group 2.

No. O. S	K	Time (sec)	$\delta_{max}$ (mm)
II.V-G2-S01	21.40	2.18E-03	8.6376
II.V-G2-S02	10.70	2.18E-03	9.3781
II.V-G2-S03	7.10	2.18E-03	10.101
II.V-G2-S04	5.40	2.18E-03	10.612
II.V-G2-S05	4.30	2.18E-03	11.027
II.V-G2-S06	3.60	2.18E-03	11.504
II.V-G2-S07	3.10	2.18E-03	12.377

NO. S (i.e., Number of Samples).



**Figure 11.** Relationship between K (i.e., stiffness modulus) &  $\delta_{max}$  (i.e., Max. deflection (mm)) of Group2.

### 5.2.3 Comparison between II.V-G1 and II.V-G2.

Figure 12. illustrates the comparison between the two groups, and as mentioned previously that the only difference between them is the type of support. Group 1 is fixed support and the second is hinged support. It was noticed that the deflection values in the group with the hinged support are less than their fixed counterpart. This is due to the presence of the hinged support in the silos, which gives it flexibility, which in turn, reduces the absorption of blast waves, in contrast to the fixed support.

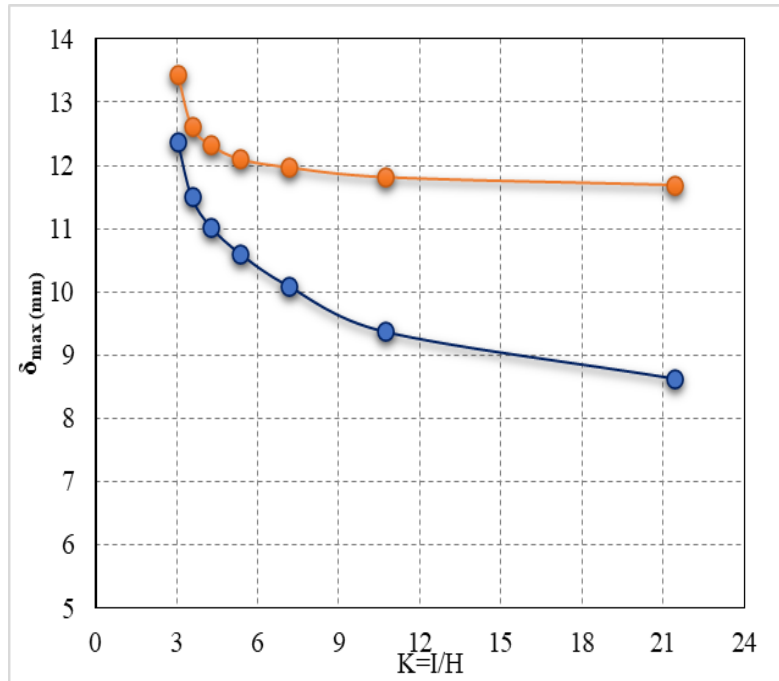


**Figure 12.** Group1 and Group 2 results for the relationship between K (i.e., stiffness modulus) &  $\delta_{\max}$  (i.e., Max. deflection (mm)).

### 5.3 Case study III. Filling & unloading.

This case was concerned with the study of the effect of the Filling & unloading of concrete silos when exposed to Blast load. The comparison points mentioned above for Group1 and Group2 are similar in rates of filling & unloading and different only in the type of support fixed and hinged respectively. Maximum deflection values for different samples of the two groups are presented below.

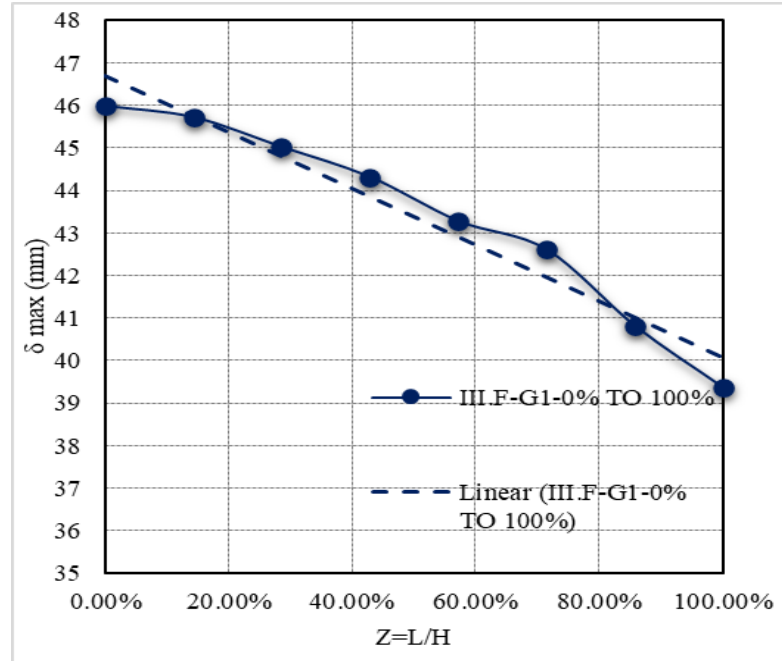
#### 5.3.1 Analysis result of III.F-G1.

Figure 13 shows the relationship between  $\delta_{\max}$  (i.e. the maximum deformation of the RC silo) and the coefficient Z (i.e. Filling rate). The values Z &  $\delta_{\max}$  have an inverse relationship due to the loading effect to the section. In this case, is the difference in pressure resulting from dynamic and static loads. The values of  $\delta_{\max}$  & Z are shown in Table 4.

**Table 4.** Values of Max. deflection  $\delta_{\max}$  & Filling factor Z Group1.

No. O. S	Z	$\delta_{\max}$ (mm)
III.F-G1-S01	0.00%	45.985
III.F-G1-S02	14.29%	45.719
III.F-G1-S03	28.57%	45.021
III.F-G1-S04	42.86%	44.315
III.F-G1-S05	57.14%	43.279
III.F-G1-S06	71.43%	42.607
III.F-G1-S07	85.71%	40.813
III.F-G1-S08	100.00%	39.36

NO. S (i.e., Number of Samples).



**Figure 13.** Relationship between  $\delta_{\max}$  (i.e., Max. deflection (mm)) & Z (i.e., Filling factor) of (III.F. Group1).

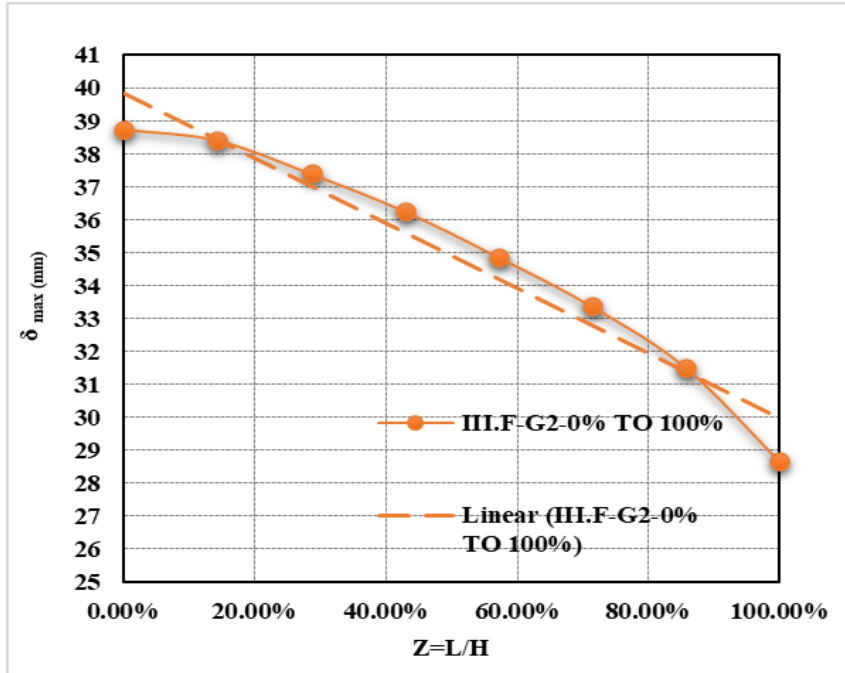
### 5.3.2 Analysis result of III.F-G2.

Figure 14 shows the relationship between  $\delta_{\max}$  (i.e. maximum deformation of an RC silo) and the coefficient Z (i.e., packing rate). The results show a similarity in that there is an inverse relationship between  $\delta_{\max}$  & Z, just as for group 1. but It was observed that the deformation values were lower than those of group 1. Therefore, the deformation results for the two groups should be compared. The values of  $\delta_{\max}$  & Z will be shown in Table 5.

**Table 5.** Values of Max. deflection  $\delta_{\max}$  & Filling factor Z Group2

No. O. S	Z	$\delta_{\max}$ (mm)
III.F-G2-S01	0.00%	38.749
III.F-G2-S02	14.29%	38.415
III.F-G2-S03	28.57%	37.403
III.F-G2-S04	42.86%	36.257
III.F-G2-S05	57.14%	34.865
III.F-G2-S06	71.43%	33.363
III.F-G2-S07	85.71%	31.503
III.F-G2-S08	100.00%	28.664

NO. S (i.e., Number of Samples).



**Figure 14.** Relationship between  $\delta_{max}$  (i.e., Max. deflection (mm)) & Z (i.e., Filling factor) of (III.F. Group2).

### 5.3.3 Comparison between III.F-G1 and III.F-G2.

Figure 15 shows a comparison between the two groups, with the sole variation being the sort of support provided, as previously stated. Support that is both fixed and hinged. As RC silos were provided flexibility through hinged support, deformation values were reduced by 16 to 27 percent when compared to the fixed support group.

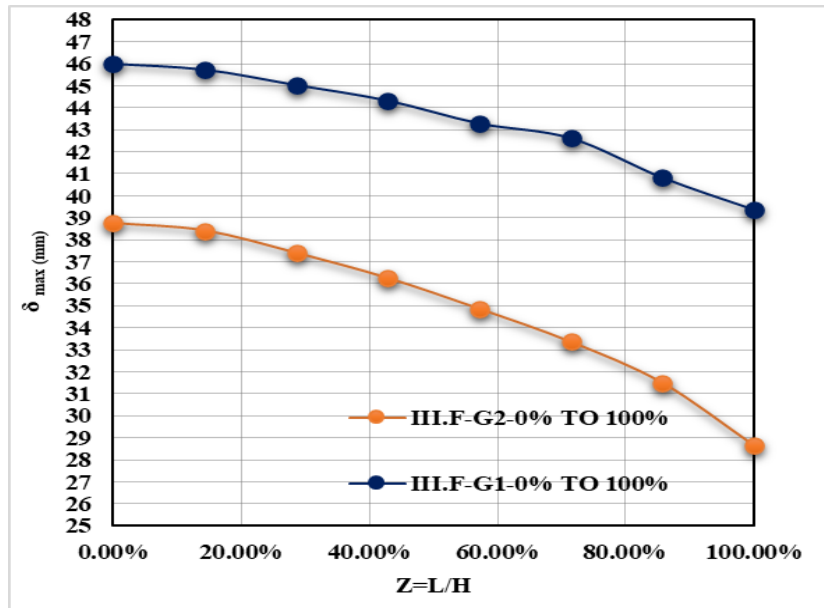


**Figure 15.** III.F. Group1 and III.F. Group 2 results for the relationship between  $\delta_{max}$  (i.e., Max. deflection (mm)) & Z (i.e., Filling factor).

## 6. Conclusion.

This study was a diligent trial to spot the light on some factors (architectural, topographic, and design factors) that can be taken into consideration to provide extra protection to strategic structures against the explosions and to define to what extent these factors can effectively decrease the damage.

The use of a more convex and curved horizontal section had a significant impact on the shape's ability to penetrate the explosion waves without the concentration of the reflected pressure on its perimeter. It was noticed that the value of the reflected pressure measured on the front face of the circular section is less than its counterpart for the rectangular section by 17.80%, and also the value measured on the front face of the diamond section is less than its counterpart for the rectangle section by 58.8%.

For the role that stiffness plays in resisting the blasting load, it was concluded that increasing stiffness is very effective for resisting blast loads when the value of (K)factor is less than 9.00 (as an average value) which decreases effectively RC silo defamation but higher than that it would not give the **desired** results i.e., it would decrease the deformation value but not as effective as the previous state. the deformation value decreases due to increasing the value of the stiffness coefficient (K) by 12.65% in the case of fixed support and by 30.21% in the case of hinged support.

Controlling the RC silo fill state, statistical speaking, so that it would be semi-full at most times would provide additional protection (according to the inverse relationship between the filling factor and the deformation of the silo that this study stated). the deformation value decreases due to increasing the value of the filling coefficient (Z) by 14.6% in the case of fixed support and by 26.00% in the case of hinged support.

Support type also has a significant effect on the deformation value. The more flexible the support is the less the deformation value gets. where the use of hinged support reduced the value of deformation by 27% nearly compared to its counterpart in the case of using fixed support.

In the future, it is possible to study other factors that may influence to provide additional protection, such as the percentage of steel within the concrete section, **and** the use of additives in concrete

## References.

- [1]. P. Smith and D. Cormie, "3 Blast loading," in *Blast effects on buildings*: Thomas Telford Publishing, 2009, pp. 30-58. [<https://doi.org/10.1680/beob2e.35218.0003>].
- [2]. G. F. Kinney and K. J. Graham, "Explosions," in *Explosive Shocks in Air*, G. F. Kinney and K. J. Graham, Eds. Berlin, Heidelberg: Springer Berlin Heidelberg, 1985, pp. 1-17. [[https://doi.org/10.1007/978-3-642-86682-1\\_1](https://doi.org/10.1007/978-3-642-86682-1_1)]
- [3]. T. Ngo, P. Mendis, A. Gupta, and J. Ramsay, "Blast loading and blast effects on structures—an overview," *Electronic Journal of Structural Engineering*, vol. 7, no. S1, pp. 76-91, 2007.
- [4]. C. Johnson, P. Mulligan, K. Williams, M. Langenderfer, and J. Heniff, "Effect of explosive charge geometry on shock wave propagation," in *AIP Conference Proceedings*, 2018, vol. 1979, no. 1, p. 150021: AIP Publishing LLC. [<https://doi.org/10.1063/1.5044977>]
- [5]. Gebbeken N, Döge T. Explosion Protection—Architectural Design, Urban Planning and Landscape Planning. *International Journal of Protective Structures*. 2010;1(1):121.[<https://doi.org/10.1260%2F2041-4196.1.1.1>]
- [6]. Králik, Juraj, and Michal Baran. "Numerical Analysis of the Exterior Explosion Effects on the Buildings with Barriers." *Applied Mechanics and Materials*, Aug. 2013, vol. 390, Trans Tech Publications, Ltd., pp. 230–234. Crossref, [<https://doi.org/10.4028/www.scientific.net/AMM.390.230>]
- [7]. Y. Temsah, A. Jahami, and C. J. E. S. Aouad, "Silos structural response to blast loading," 2021, vol. 243, p. 112671. [<https://doi.org/10.1016/j.engstruct.2021.112671>]
- [8]. M. Chiquito, A. P. Santos, L. M. López, and R. Castedo, "Blast Effects on Structural Elements", in *Fracture Mechanics Applications*. London, United Kingdom: IntechOpen, 2019 [Online]. Available: <https://www.intechopen.com/chapters/68578> doi: 10.5772/intechopen.88721
- [9]. Schenker A, Anteby I, Gal E, Kivity Y, Nizri E, Sadot O, Michaelis R, Levintant O, Ben-Dor G. Full-scale field tests of concrete slabs subjected to blast loads. *International Journal of Impact Engineering*. 2008 Mar 1;35(3):184-98. [<https://doi.org/10.1016/j.ijimpeng.2006.12.008>]
- [10]. Ismail, Sahar Ali, Raphael, Wassim, Durand, Emmanuel, Kaddah, Fouad, Geara, Fadi Analysis of the structural response of Beirut port concrete silos under blast loading. *Archives of Civil Engineering*. 2021, 67s. 619–638. [<https://doi.org/10.24425/ace.2021.138074>]
- [11]. Hetherington J, Smith P. "Blast waves and blast loading" in *Blast and ballistic loading of structures*. Hetherington J, Smith P., 1st Edition. CRC Press; 2014 Apr 21, 39 [<https://doi.org/10.1201/9781482269277>.]
- [12]. ASCE, "Blast protection of buildings: ASCE/SEI 59-11," 2011.[<https://doi.org/10.1061/9780784411889>.]

- [13]. Needham C.E. Formation of Blast Waves. In: Blast Waves. Shock Wave and High Pressure Phenomena. Springer, Cham,(2018). [[https://doi.org/10.1007/978-3-319-65382-2\\_4](https://doi.org/10.1007/978-3-319-65382-2_4)]
- [14]. D. o. Defense, Unified Facilities Criteria (UFC): Structures to Resist the Effects of Accidental Explosions (UFC 3–340–02), Change 2, 1 ed. Departments of the Army, the Navy, and the Air Force Washington, DC, 2008.[ [http://dod.wbdg.org/.](http://dod.wbdg.org/)]
- [15]. F. G. Friedlander, The wave equation on a curved space-time. Cambridge university press, 1975.vol.2
- [16]. E. Lee, H. Hornig, and J. Kury, "Adiabatic expansion of high explosive detonation products," Univ. of California Radiation Lab. at Livermore, Livermore, CA (UnitedStates)1968.[[https://doi.org/10.2172/4783904.](https://doi.org/10.2172/4783904)]
- [17]. Y. Han, X. Xie, Z. Jiang, Y. Duan, and Y. Wen, "Equation of state of detonation products for TNT by aquarium experiment," in AIP Conference Proceedings, 2018, vol. 1979, no. 1, p. 100016: AIP Publishing LLC. [[https://doi.org/10.1063/1.5044888.](https://doi.org/10.1063/1.5044888)]
- [18]. G. F. C. Rogers and Y. R. Mayhew, Thermodynamic and transport properties of fluids. John Wiley & Sons, 1995.[online] [https://www.wiley.com/en-gb/Thermodynamic+and+Transport+Properties+of+Fluids%2C+5th+Edition-p-9781119848981.](https://www.wiley.com/en-gb/Thermodynamic+and+Transport+Properties+of+Fluids%2C+5th+Edition-p-9781119848981)
- [19]. Herrmann W. Constitutive equation for the dynamic compaction of ductile porous materials. Journal of applied physics. 1969 May;40(6):2490-9. [[https://doi.org/10.1063/1.1658021.](https://doi.org/10.1063/1.1658021)]
- [20]. Riedel W, Kawai N, Kondo KI. Numerical assessment for impact strength measurements in concrete materials. International Journal of Impact Engineering. 2009 Feb 1;36(2):283-93. [[https://doi.org/10.1016/j.ijimpeng.2007.12.012.](https://doi.org/10.1016/j.ijimpeng.2007.12.012)]